Available online at www.sciencedirect.com
SCIENCE DIRECT®
International Journal of Pharmaceutics 305 (2005) 129–144
international journal of pharmaceutics
www.elsevier.com/locate/ijpharm

Pharmaceutical Nanotechnology

NMR characterization of paclitaxel/poly (styrene-isobutylene-styrene) formulations

Jian-Zhong Chen [a,b], Shrirang V. Ranade [c,**], Xiang-Qun Xie [a,b,*]

[a] *Department of Pharmaceutical & Pharmacological Sciences, College of Pharmacy, University of Houston, Houston, TX 77204, USA*
[b] *Institute of Materials Science and Department of Pharmaceutical Sciences, School of Pharmacy, University of Connecticut, Storrs, CT 06269, USA*
[c] *Corporate Research & Advanced Technology Development, Boston Scientific Corporation, Natick, MA 01760, USA*

Received 16 June 2005; received in revised form 16 August 2005; accepted 18 August 2005
Available online 3 October 2005

Abstract

TAXUS™ is a coronary drug-eluting stent system utilizing a formulation consisting of cellular-target drug paclitaxel and poly (styrene-isobutylene-styrene) (SIBS). The present study investigates the interaction and interfacial dynamics of paclitaxel incorporated in a nano-polymeric matrix system. Solution and solid-state CP/MAS NMR experiments were designed to characterize the microstructure of heterogeneous drug–polymer mixtures in terms of its composition, molecular mobility, molecular order, paclitaxel–SIBS molecular interactions, and molecular mobility of the drug in the polymer matrix. The NMR spectra demonstrated unchanged chemical shifts between the neat and incorporated paclitaxel, and suggested that the level of the interactions between paclitaxel and SIBS is limited to non-bonding interactions or physical interactions between paclitaxel and SIBS when mixed in solution under NMR detection. Carbon spin-lattice relaxation time and proton spin-lattice relaxation time in the rotating frame offer further confirmation that the mobility of paclitaxel is increased in the paclitaxel–SIBS mixture. The results also indicate that a change occurs from crystalline packing to amorphous packing in paclitaxel due to its intermolecular interaction with SIBS. Our studies were used in understanding the detailed structure, morphology, and molecular motion of paclitaxel in the paclitaxel–SIBS system and to probe chemical and physical heterogeneity down to the nanometer scale.

Keywords: Paclitaxel; Poly (styrene-isobutylene-styrene) (SIBS); Solid-state NMR; Drug–polymer interactions

1. Introduction

The polymer carrier technology in the TAXUS™ drug-eluting stent consists of a thermoplastic elastomer poly (styrene-*b*-isobutylene-*b*-styrene) (SIBS) with micro-phase separated morphology resulting in optimal properties for a drug delivery stent coating.

* Corresponding author. Tel.: +1 713 743 1288.
** Corresponding author.
E-mail addresses: shrirang_ranade@hotmail.com (S.V. Ranade), xxie@uh.edu (X.-Q. Xie).

0378-5173/$ – see front matter © 2005 Elsevier B.V. All rights reserved.
doi:10.1016/j.ijpharm.2005.08.010

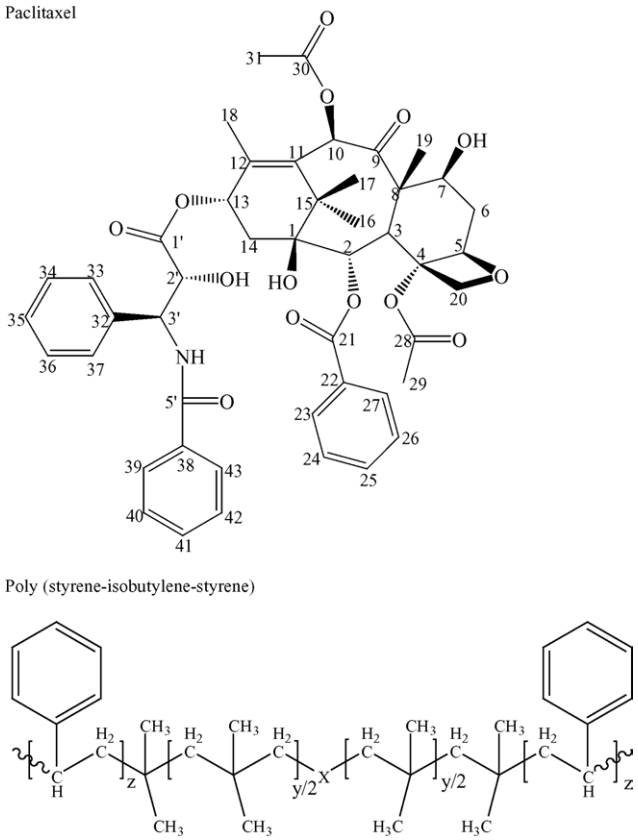

Fig. 1. Chemical structures of paclitaxel (top) and poly (styrene-isobutylene-styrene) (bottom).

Comprehensive physical characterization of the stent coatings and cast film formulations showed that paclitaxel exists primarily as discrete nano-particles embedded in the SIBS matrix (Ranade et al., 2004, 2005). The TAXUS^{TM} coronary stent system consists of two materials, paclitaxel and SIBS, as shown in Fig. 1. Paclitaxel (an anti-cancer drug) is incorporated within the polymeric matrix in solution and then deposited as a coating onto a stainless steel stent. The stent is a medical device used to treat arteriosclerosis; drug-eluting stents are used to treat restenosis. Paclitaxel is a structurally complex molecule (Schiff et al., 1979; Guenard et al., 1993a). SIBS is a thermoplastic elastomer; a triblock copolymer (Storey et al., 1994) containing a mid-segment of rubber (polyisobutylene, PIB) flanked by glassy outer segments of polystyrene (PS). Previous studies did not detect any evidence of solubility of paclitaxel in SIBS or of any molecular miscibility between paclitaxel and SIBS by DSC, DMTA or microscopy (Ranade et al., 2004).

The clinical performance of the TAXUS^{TM} stent system has been described elsewhere (Grube et al., 2003; Chieffo and Colombo, 2004; Stone et al., 2004a,b). Paclitaxel is a naturally occurring lipophilic drug that was originally extracted from the pacific yew tree *Taxus brevifolia*. The drug interferes with microtubule function and results in primary and post-mitotic G_1 arrest in smooth muscle cells, thereby inhibiting proliferation of these cells without inducing apoptosis, or cell death (Belotti et al., 1996; Blagosklonny et al., 2004; Jordan and Wilson, 2004). These findings support that stent-based delivery of low doses of paclitaxel is cytostatic but not cytotoxic (Jordan et al., 1993; Blagosklonny et al., 2004; Jordan and Wilson, 2004).

High resolution solid-state NMR is an ideal method to characterize the microstructure of heterogeneous

polymer systems (Schmidt-Rohr, 1995; Neagu et al., 2000). ^{13}C NMR, using crossing polarization (CP) (Hartmann and Hahn, 1962; Pines et al., 1973) and magic-angle spinning (MAS) (Andrew, 1981), is an important analytical tool for the solid-state characterization of polymers (Schaefer et al., 1977; Sullivan and Maciel, 1982). NMR spectroscopy applied to solid materials leads to valuable information regarding composition, molecular mobility, and molecular order. It is therefore capable of probing chemical or physical heterogeneities down to a scale below 1 nm (Schmidt-Rohr, 1995). Additionally, this method has the advantage of retrieving information about phase separation in a non-invasive manner and without any sample modification. Hence, it could also use samples taken directly from the industrial stream to be analyzed without any further modification. Solid-state NMR can determine, simultaneously, domain sizes and interface thickness (Neagu et al., 2000).

Furthermore, since solid-state NMR can be used to study the characterization of pharmaceutical solids including drug substance and dosage form, it has been become an integral technique in the field of pharmaceutical sciences (Tishmack et al., 2003). For example, Grant and co-workers (Harper et al., 2002, 2005) applied solid-state NMR to study paclitaxel polymorphs. Paclitaxel is a structurally complex molecule important in chemistry, biology, and medicine. Li et al. (2000) used fluorescence and solid-state NMR spectroscopy to examine the conformation of microtubule-bound paclitaxel.

In this work, solution and solid-state CP/MAS NMR experiments were designed to characterize the microstructure of heterogeneous drug–polymer mixtures. Also in this work, experiments were designed to characterize the microstructure of paclitaxel incorporated in SIBS, in terms of its composition, molecular mobility, and molecular order, as well as drug–polymer molecular interactions (if any) and drug molecular mobility in the polymer matrix.

2. Experimental methods

2.1. Solution NMR samples and 1D/2D NMR experiments

Paclitaxel and SIBS (Fig. 1) were supplied by Boston Scientific Corporation. Their physical–chemical characterization has been described in detail elsewhere (Ranade et al., 2004, 2005, and references therein). The following four samples were prepared for liquid state NMR experiments: (a) 12.2 mg paclitaxel in 0.6 ml $CDCl_3$; (b) 60 mg paclitaxel in 0.6 ml $CDCl_3$; (c) 60 mg:60 mg of paclitaxel/SIBS (1:1, w/w) in 0.6 ml $CDCl_3$; (d) 60 mg:120 mg of paclitaxel/SIBS (1:2, w/w) in 0.6 ml $CDCl_3$. Chemical shifts are referenced to tetramethylsilane (TMS) for ^1H and to solvent peak for ^{13}C.

The NMR measurements were carried out on a Bruker AVANCE DMX500 spectrometer. The experiments were carried out including: 1D proton, 1D carbon, 2D COSYDQF, 2D HMQC, and 2D HMBC. These experiments were designed to assign chemical shifts and allow detection of chemical shift changes between pure components and the paclitaxel–SIBS mixture.

^{13}C T_1 relaxation can provide an approach to measure atomic-level dynamic behavior of molecules in solution, and has served as an important tool for evaluating the internal dynamics of small molecules and large macromolecules (Voelker, 1991). In solution state, the spin-lattice (T_1) relaxation time of the various ^{13}C nuclei of a molecule may be determined by using inversion recovery experiments. It is important to use inverse-gated ^1H decoupling to improve the spectral signal-to-noise ratio without selectively enhancing peak intensities through NOE effects. In our experiments, ^{13}C T_1 inversion recovery experiment was carried out at 125 MHz with data acquisition 96 scans, pulse delay 20.0 s, variable delays 0.01 s, 0.05 s, 0.1 s, 0.5 s, 1.0 s, 2.0 s, 4.0 s, 7.0 s, 10 s, 14 s, 17 s, 20 s, 24 s, 27 s, 30 s, and 40 s. T_1 calculation was done by using Bruker Xwinnmr built-in macro program.

2.2. Solid-state NMR samples and ^{13}C CP/MAS experiments

NMR sample (paclitaxel–SIBS, 1:2, w/w) was prepared by first dissolving 60 mg of paclitaxel and 120 mg of SIBS in 0.6 ml of chloroform separately, then mixing paclitaxel solution into SIBS solution, and subsequently drying out the solvent under dry N_2 gas. A thin film of the mixed sample was formed on the glass wall of the small vial and it was subjected to vacuum pump for 48 h to remove the residual solvent from the sam-

ple. Such paclitaxel–SIBS formations were evaluated as cast films to facilitate sample preparation for NMR (Ranade et al., 2004). All samples were packed in 5 mm zirconia pencil sample rotors. All sample preparations described above were performed in a fume hood. The following three NMR samples were prepared for solid-state NMR experiments: (a) neat paclitaxel, (b) neat SIBS, and (c) paclitaxel–SIBS mixture (1:2, w/w).

High power proton decoupling ^{13}C CP/MAS NMR spectra were recorded at 75 MHz, using a Chemagnetics CMX300 NMR spectrometer with a commercial double-bearing 5.0 mm MAS probe. The magic angle was set using the ^{79}Br resonance of KBr. Samples (∼100 mg) were packed in zirconia pencil rotors and spun at the magic angle at 10 kHz. The 90° pulse widths for ^{13}C were 4.14 μs. A relaxation time of 2 s was used to allow thermal equilibrium, and 2048 or 10,240 acquisitions were utilized to achieve an adequate signal–noise ratio. A 76 kHz proton decoupling field was used during the acquisition of the free induction decay. ^{13}C spectra were recorded using cross-polarization that improves sensitivity by transferring magnetization from ^{1}H to ^{13}C (a typical contact time, 1.5–5 ms). The Hartmann–Hahn match condition for ^{13}C was set experimentally using the ^{13}C labeled glycine standard. Chemical shifts are given with respect to TMS for using an external sample of solid glycine (176.03 ppm) for ^{13}C.

Carbon spin-lattice relaxation time (^{13}C T_{1xCP}) measurement was carried out by using CP-version T_1 pulse program with acquisition parameters similar to a regular CP/MAS experiments: contact time 1.5 ms, pulse delay 2 s, acquisition scan 4096, magic-angle spinning rate 10 kHz, and temperature 298 K. Experiments in which relaxation period τ is varied give a set of data from which the ^{13}C T_{1xCP} value can be obtained by analysis.

Proton spin-lattice relaxation time in rotating frame ($T_{1\rho H}$) values were measured through detecting carbon atoms by inserting a variable proton spin-lock period before the contact with the carbons is made. A normal cross-polarization pulse sequence is utilized while inserting a variable ^{1}H spin-lock time, a relaxation time period with length of τ incrementing from 0.01 ms to 25 ms, and proton decoupling power (76 kHz), at the beginning of the contact period at which time the Hartmann–Hahn condition is established. During the time period τ, the rotating frame ^{1}H spin-lattice relaxation occurs; hence, by observing the ^{13}C intensity at the end of the contact period as a function of τ one can obtain a measure of $T_{1\rho H}$. $T_{1\rho H}$ values were calculated using curve-fitting analysis of variable proton spin-lock time data with standard deviation less than 8% and a correlation coefficient, $R^2 > 0.9$.

3. Results and discussion

3.1. High-resolution NMR study of paclitaxel–SIBS interactions in solution

3.1.1. Chemical shift assignments

The proton and carbon signal assignments for both paclitaxel and SIBS were done by 2D 1H-1H COSY-DQF, ^{1}H-^{13}C HMQC, and were then confirmed by ^{1}H-^{13}C HMBC experiments (data not shown). The results corroborate data reported in the literature (Chmurny et al., 1992; Moyna et al., 1997). Table 1 summarizes the ^{13}C and ^{1}H chemical shifts of neat paclitaxel and paclitaxel–SIBS mixture in $CDCl_3$. The process of accurately assigning chemical shifts for the targeted compounds is necessary to enable interpretation of solid-state NMR data later.

Chloroform was chosen as the solvent since it provides a non-polar environment similar to the hydrophobic polymer matrix (SIBS). In addition, a non-polar solvent avoids the complications introduced by solvent–sample interactions. Both paclitaxel and SIBS have acceptable solubility in chloroform, which allows the preparation of the paclitaxel–SIBS sample mixture. The sample containing a high ratio of paclitaxel was prepared in order to generate measurable paclitaxel signals in paclitaxel/SIBS mixture by NMR experiments. The detectable paclitaxel proton and carbon signals are particularly critical for the later solid-state NMR experimental studies that were designed to probe the paclitaxel/SIBS interactions in the solid state. The experimental design, 1:1 or 1:2 (w/w) ratios of paclitaxel/SIBS, ensured that both solution and solid-state NMR experiments provided accurate and sensitive signals for the mixture (paclitaxel/SIBS) samples. Furthermore, it is reasonable to make an assumption that if there is no detectable chemical interaction between paclitaxel and SIBS in 1:1 or 1:2 (w/w) ratios then the preparation of the 1:3 (w/w) ratio of paclitaxel/SIBS mixture can be excluded.

Table 1
^{13}C and ^{1}H chemical shifts and ^{13}C T_1 measurements of paclitaxel in $CDCl_3$ and paclitaxel–SIBS mixtures in $CDCl_3$

Carbons	60 mg Paclitaxel in $CDCI_3$			60:60 mg Paclitaxel:SIBS		60:120 mg Paclitaxel:SIBS in $CDCI_3$		
	^{13}C (ppm)	^{13}C T_1 (ms)	^{1}H (ppm)	^{13}C (ppm)	^{1}H (ppm)	^{13}C (ppm)	^{13}C T_1 (ms)	^{1}H (ppm)
C-9	203.57	1.387		203.57		203.57	1.124	
C-28	170.33	1.467		170.34		170.35	1.211	
C-30	171.18	1.59		171.18		171.17	1.163	
C-1′	172.63	1.506		172.65		172.66	1.113	
C-5′	166.87	1.63		166.85		166.84	–	
C-11	133.07	1.284		133.07		133.08	1.065	
C-12	141.88	1.067		141.86		141.86	1.102	
C-21	167.14	1.954		167.18		167.2	1.791	
C-22	129.1	1.56		129.13		129.15	1.312	
C-23, 27	130.13	0.293	8.11	130.13	8.11	130.15	0.27	8.11
C-24, 26	128.66	0.313	7.49	128.66	7.49	128.66	0.4	7.48
C-25	133.64	0.351	7.6	133.64	7.59	133.62	0.32	7.58
C-32	133.58	0.284		133.58		133.58	0.317	
C-33, 37	127.02	0.835	7.46	127.03	7.46	127.04	0.75	7.46
C-34, 36	128.92	0.709	7.37	129.91	7.36	128.91	0.612	7.35
C-35	128.25	0.352	7.33	128.23	7.33	128.23	0.312	7.32
C-38	137.94	1.543		137.95		137.98	1.313	
C-39, 43	126.98	0.74	7.73	126.98	7.72	126.99	0.584	7.72
C-40, 42	128.6	0.757	7.4	128.6	7.39	128.6	0.7	7.39
C-41	131.88	0.371	7.47	131.88	7.47	131.87	0.317	7.46
C-1	78.88	3.002		78.86		78.86	3.104	
C-2	74.89	0.306	5.66	74.89	5.66	74.91	0.247	5.66
C-3	45.61	3.109	3.78	45.61	3.78	45.64	3.128	3.78
C-4	81.04	0.366		81.04		81.05	0.395	
C-5	84.33	–	4.92	84.33	4.92	84.33	–	4.91
C-6	35.62	0.315	2.51, 1.85	35.62	2.51, 1.85	35.62	0.316	2.50, 1.85
C-1	72.06	3.451	4.38	72.05	4.38	72.05	3.728	4.38
C-8	58.47	0.362		58.46		58.46	0.327	
C-10	75.51	0.389	6.27	75.52	6.27	75.53	0.29	6.27
C-13	72.15	–	6.2	72.14	6.2	72.13	–	6.2
C-14	35.58	3.756	2.32, 2.27	35.6	2.31, 2.27	35.62	4.034	2.31, 2.27
C-15	43.09	1.412		43.09		43.1	–	
C-17	26.76	0.2	1.22	26.76	1.21	26.76	0.26	1.21
C-16	21.75	1.049	1.12	21.76	∼	21.77	2.396	∼
C-18	14.75	0.639	1.67	14.75	1.67	14.75	0.534	1.67
C-19	9.52	0.201	1.78	9.53	1.78	9.55	0.146	1.78
C-20	76.42	1.629	4.28, 4.18	76.41	4.28, 4.18	76.42	1.966	4.27, 4.18
C-29	22.53	1.474	2.36	22.53	2.36	22.54	1.618	2.36
C-31	20.8	0.378	2.21	20.8	2.2	20.81	0.362	2.19
C-2′	73.16	0.355	4.77	73.15	4.77	73.16	0.375	4.77
C-3′	55.06		5.76	55.08	5.76	55.09		5.76
$C_{2'}$–OH			3.84		3.9			3.94
C_1–OH			1.98		2.04			2.06
C_7–OH			2.56		2.6			2.61
N–H			7.11		∼			∼

(∼) The peak is overlapped with the peak from SIBS.

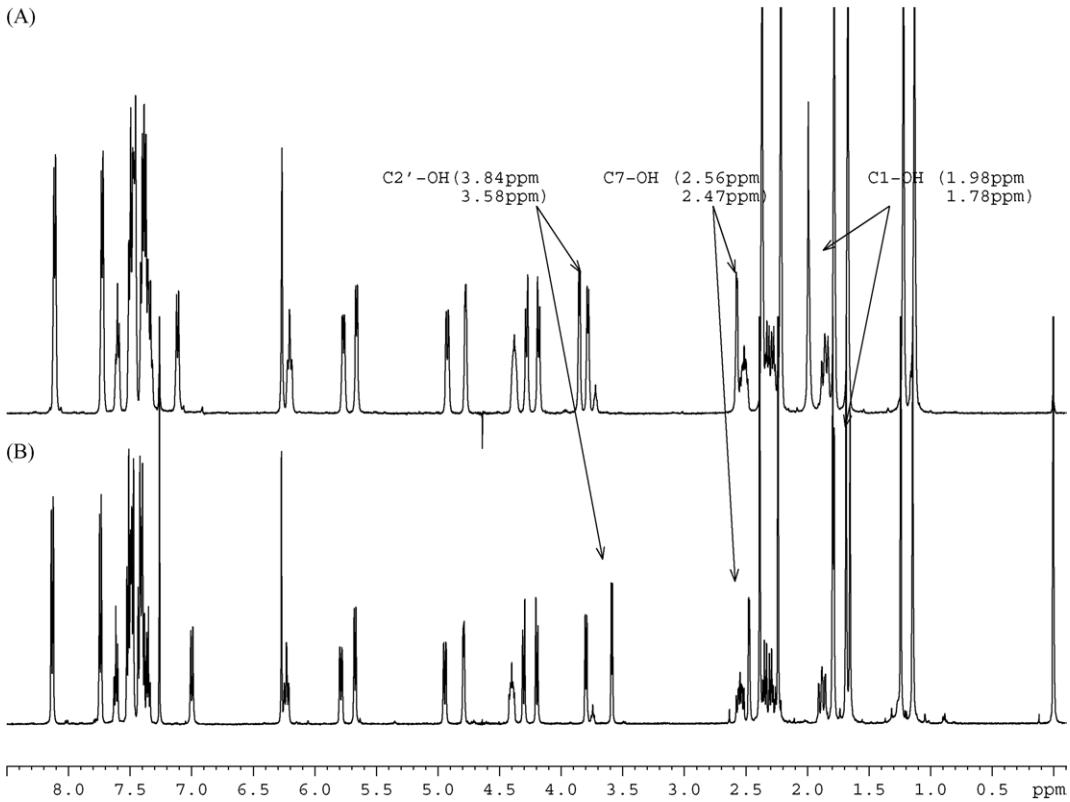

Fig. 2. ^{1}H 500 MHz spectra of paclitaxel in $CDCl_3$ at concentrations of 100 mg/ml (A) and 20.3 mg/ml (B) at 298 K.

3.1.2. Comparison of chemical shift changes

These studies were designed to detect possible changes in the chemical shift of paclitaxel before and after incorporation into the SIBS matrix. The information provided an understanding of: (i) types of interaction between paclitaxel and SIBS, if any; (ii) chemical reaction among the two, if any; (iii) detection of new species that may be formed under different concentrations.

Fig. 2 shows the concentration-dependent study of neat paclitaxel sample in $CDCl_3$ at 298 K. Solution ^{1}H NMR spectra (Fig. 2) show that the proton signals of paclitaxel retain the same chemical shifts except the three OH protons. The three OH protons shifted up-field ($C_{2'}$–OH, 0.26 ppm; C_1–OH, 0.20 ppm; C_7–OH, 0.09 ppm) when the sample was diluted from a concentration of 100 mg/ml to 20.3 mg/ml. The result is as expected since this is a typical NMR detection of the phenomenon of intermolecular hydrogen bonding of the OH groups. The crystal structure of paclitaxel indicates that these three OH protons form intermolecular hydrogen bonding (Mastropaolo et al., 1995).

When the paclitaxel was mixed with SIBS in $CDCl_3$ solution, we anticipated observing an up-field shift similar to the dilution effect on the hydroxyl groups in paclitaxel since SIBS may act as another “solvent” to “dilute” paclitaxel. However, our results showed the opposite (Fig. 3), a down-field shifting of the chemical shifts for the three OH groups. The proton resonance of the three OH groups shifted down-field ($C_{2'}$–OH, 0.10 ppm; C_1–OH, 0.08 ppm; C_7–OH, 0.05 ppm). A possible interpretation is that adding SIBS solution was not just like adding a solvent to dilute the concentration of paclitaxel. Instead, paclitaxel molecules interrupted the SIBS polymer chain packing through π–π interaction of aromatic ring structures between the two compounds. This was also confirmed by the evidence of the relatively larger proton signal down-field shift for $C_{2'}$–OH (0.10 ppm) and C_1–OH (0.08 ppm) than C_7–OH (0.05 ppm) since C_7–OH is farther away

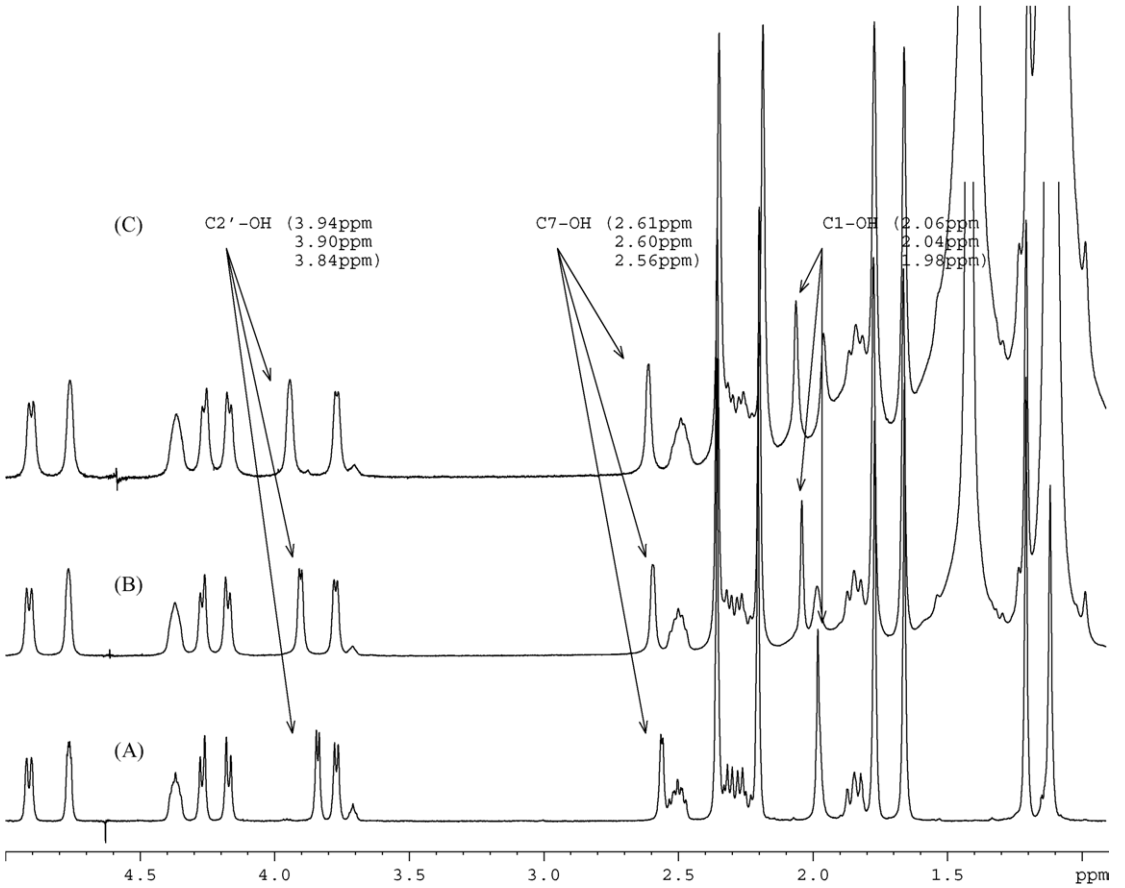

Fig. 3. Stack plot (up-field region) of ^{1}H 500 MHz spectra of neat paclitaxel (A), paclitaxel–SIBS mixture (1:1, w/w) (B), and paclitaxel–SIBS mixture (1:2, w/w) (C) in $CDCl_3$ at 298 K.

from aromatic side chains of paclitaxel molecules. We hypothesize that the signal down-field shift of $C_{2'}$- and C_1–OH groups may be attributed to the aromatic side-chain interactions between paclitaxel and SIBS. Such non-bonded aromatic π–π interaction disrupts the side-chain conformations of the paclitaxel molecule, resulting in the down-field shift of the $C_{2'}$- and C_1–OH proton signals.

Again, our data revealed that only physical or non-bonding interactions occurred in mixing paclitaxel and SIBS in solution, and in addition, the chemical shift changes of hydroxyl groups indicated that the interaction is limited to non-bonded van der Waals interaction between the two molecules in solution.

3.1.3. Comparison of spin-lattice relaxation (T_1) changes

Fig. 4 shows stacked spectra of the ^{13}C T_1 relaxation time measured by inversion recovery experiments for paclitaxel–SIBS (1:2, w/w) mixture in $CDCl_3$. Table 1 summarizes the ^{13}C T_1 values of pure paclitaxel and paclitaxel–SIBS mixtures (1:2, w/w) in $CDCl_3$. The experiments were designed to probe the molecular mobility of free paclitaxel and SIBS-bound paclitaxel molecules, which provided further evidence of paclitaxel–SIBS interactions.

As shown in Table 1, different ^{13}C T_1 values detected between pure paclitaxel and paclitaxel–SIBS samples indicate that the motion of paclitaxel molecules is relatively restricted due to the interac-

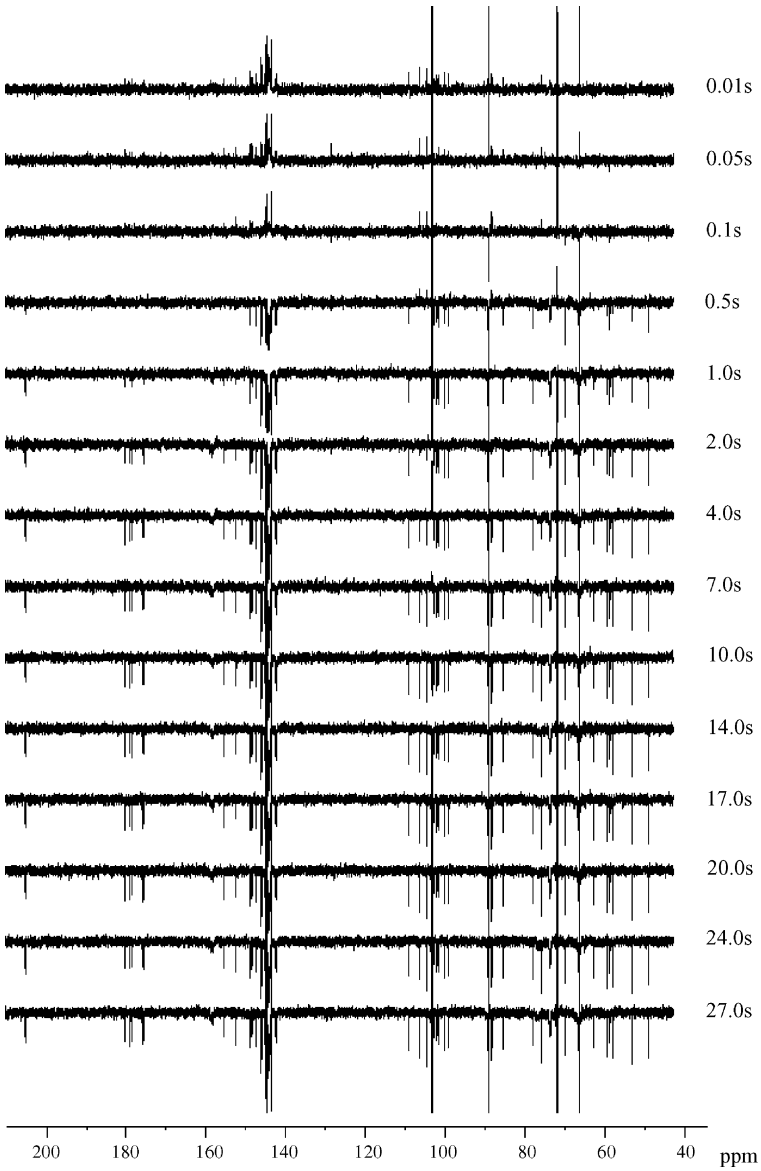

Fig. 4. Stack plot of solution NMR ^{13}C inversion recovery T_1 relaxation spectra for paclitaxel–SIBS mixture (1:2, w/w) in $CDCl_3$ at 298 K.

tion between paclitaxel and SIBS in the mixture. The decreases in T_1 values revealed the mobility changes of paclitaxel molecule due to the change from the free to the SIBS-bound states. The increases in T_1 values were observed for methyl groups (C_{16}, C_{18}, C_{29}, and C_{31}) which are attributed to the intramolecular dynamic process or free rotation of the methyl groups. The ^{13}C T_1 relaxation data may be used, in a qualitative fashion, to describe the relative flexibility of ^{13}C–^{1}H vectors of paclitaxel molecule when bound to a macromolecule. In general, it can be approximated that relatively shorter ^{13}C T_1 values are indicative of less mobile ^{13}C–^{1}H bond vectors for a small molecule in solution (Zhu et al., 1999; LaPlante et al., 2000).

In summary, ^{1}H and ^{13}C comparison studies of paclitaxel and of the paclitaxel–SIBS mixture show

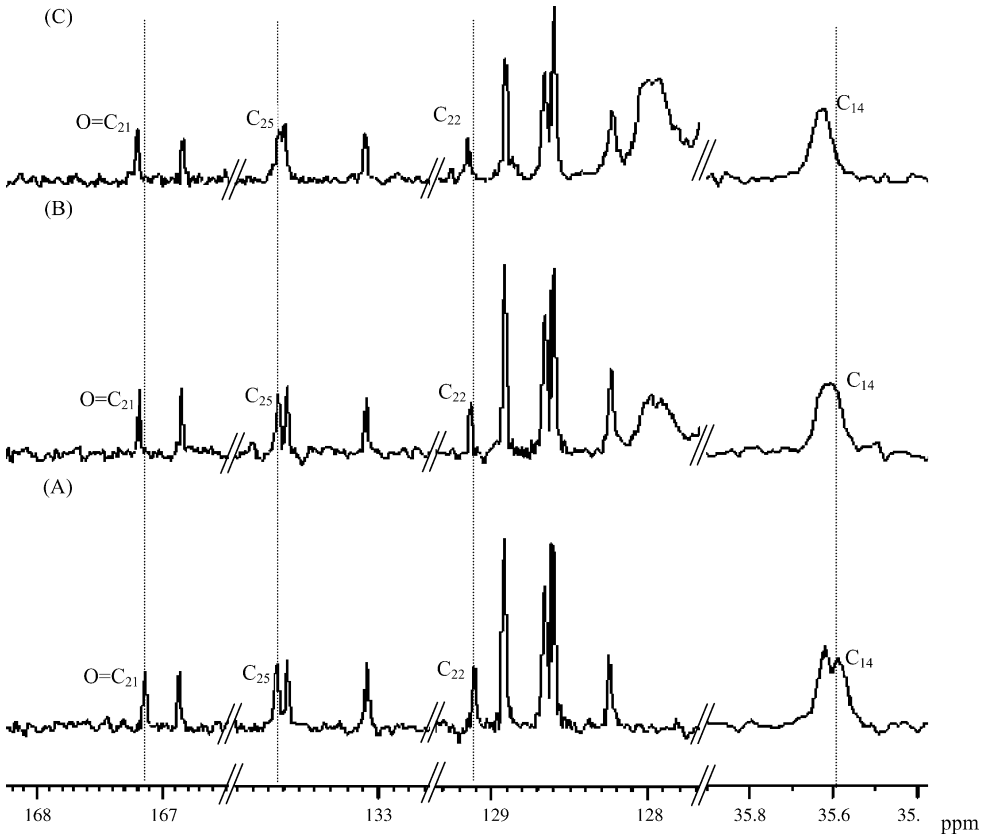

Fig. 5. Stack plot of solution ^{13}C spectra of (A) paclitaxel in $CDCl_3$, (B) paclitaxel–SIBS mixture (1:1, w/w) in $CDCl_3$, and (C) paclitaxel–SIBS mixture (1:2, w/w) in $CDCl_3$ at 298 K.

that most of the paclitaxel ^1H and ^{13}C peaks retain unchanged chemical shifts. The results indicate that the level of the interactions between paclitaxel and SIBS are limited to non-bonded or physical interactions occurring between paclitaxel and SIBS when mixed in solution. In addition, we observed some limited chemical shift changes for the certain carbon signals: C_{14} (0.04 ppm down-field), C_{21} (0.06 ppm down-field), C_{22} (0.05 ppm down-field), and C_{25} (0.02 ppm up-field) (Fig. 5). Such small changes indicate that the side-chain π–π interaction between paclitaxel and SIBS may influence the electronic environment of the sites near the C_{14} carbon and the C_2 constituent. Several studies (Guenard et al., 1993b; Chen et al., 1993) have also reported the important role of the C_2 benzoate group for biological activity.

3.2. ^{13}C CP/MAS NMR study of paclitaxel–SIBS in solid-state

CP/MAS NMR experiments were designed to explore the paclitaxel–SIBS interactions in solid state in terms of chemical shift changes, nuclear spin diffusion, rotating frame relaxation rates, and to compare these to observations made in solution.

3.2.1. Comparison of solution and solid-state NMR spectra

Fig. 6 shows a comparison of 1D ^{13}C NMR spectra of paclitaxel molecules acquired in solution and solid states. Chemical shift assignments of solid-state ^{13}C NMR spectra were made on the basis of solution NMR data. In order to easily interpret the spectra later, we classified the spectrum into five regions: (i) Region I:

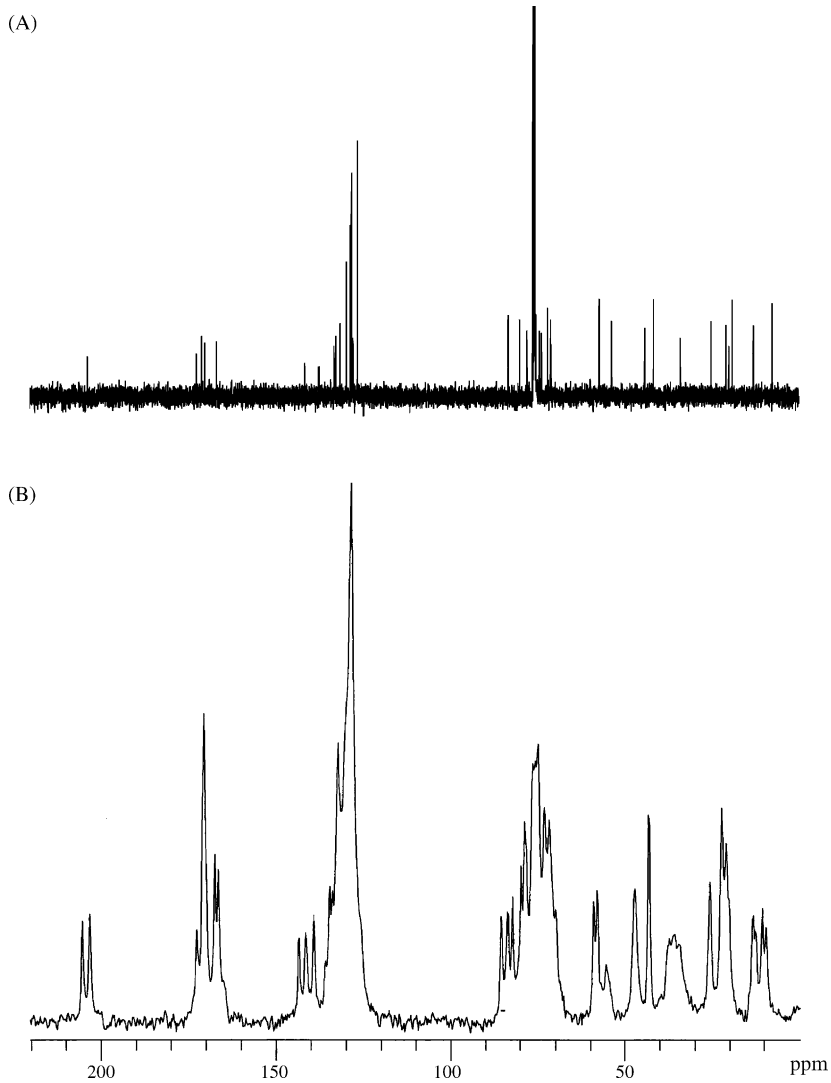

Fig. 6. ^{13}C NMR spectra of (A) paclitaxel in $CDCl_3$ solution (solution NMR) and (B) solid-state paclitaxel CP/MAS NMR measured at 298 K with 2048 acquisitions and a magic-angle spin-rate of 10 kHz.

the carbonyl carbons (>160 ppm); (ii) Region II: the aromatic or double bond carbons (140–120 ppm); (iii) Region III: the fused ring carbons or carbons adjacent to carbonyl group (86–70 ppm); (iv) Region IV: other fused ring carbons (60–30 ppm); (v) Region V: the methyl group carbons (<30 ppm).

The solid-state NMR spectral pattern (Fig. 6) reflects the anisotropic motion of solid crystalline paclitaxel, and reveals structural information beyond that available from the solution spectrum. In particular, the double ^{13}C peak pattern in solid state indicates a rigid crystalline packing for paclitaxel. For example, the carbonyl C_9 resonance (203.57 ppm) is split into two major peaks, indicating a non-equivalent molecular environment in the unit cell or conformational effects in a rigid crystal packed molecule. The reported X-ray crystal structure of paclitaxel (Mastropaolo et al., 1995) has two molecules per unit cell. The two paclitaxel molecules in the unit cell have different C-13 side-chain conformations. The peak splitting observed here can be

attributed to non-equivalence of two conformations in the crystalline paclitaxel.

3.2.2. Comparison studies of paclitaxel, SIBS, and their mixture

Fig. 7 shows a stack plot for the ^{13}C CP/MAS spectra of (A) SIBS, (B) paclitaxel, and (C) mixture (1:2, w/w) paclitaxel–SIBS. The ^{13}C CP/MAS NMR spectrum of SIBS (Fig. 7A) shows improved spectral quality to that reported upon removing the spinning side band (SSB) (Neagu et al., 2000). The broad line-width indicates the larger size and slower motion of the SIBS molecule. The spectrum is consistent with that reported by Neagu showing two CP/MAS spectra for the different compositions of the SIBS polymer.

Fig. 7B shows sharp and well-resolved peaks for paclitaxel, indicating a typical small molecule whereas SIBS shows broad peak patterns except three sharp peaks (60 ppm, 40 ppm, and 31 ppm) attributed to the polyisobutylene block in the copolymer. Comparing spectra (A) with (B) in Fig. 7, there are three broad peak regions, 140–150 ppm, 120–135 ppm, and 35–55 ppm, which tend to overlap with each other in the paclitaxel–SIBS mixture spectrum (Fig. 7B and C). Comparing (B) with (C) in Fig. 7, the ^{13}C spectrum of the paclitaxel–SIBS (1:2, w/w) mixture shows that spectral intensity and resolution of the paclitaxel peaks were dramatically decreased due to the presence of larger size and lower mobility of polymer molecules in the mixture and also due to lower molar ratio of paclitaxel in the mixture.

3.2.3. Carbon spin-lattice relaxation time (T_1) and proton spin-lock relaxation time ($T_{1\rho H}$) measurements

The solid-state CP-version ^{13}C spin-lattice relaxation time experiment T_1 (^{13}C) was designed to measure changes in mobility of paclitaxel in the free and polymer-mixed states. Table 2 summarizes the chemical shifts and CP-version inversion recovery T_1 (^{13}C) time measurements of paclitaxel, SIBS and their mixture (1:2, w/w). Due to the peak overlap in paclitaxel and SIBS spectra in two regions 30–50 ppm and 120–150 ppm, it is difficult to identify an appropriate peak for ^{13}C T_1 calculations for paclitaxel molecule in the mixture even with deconvolution of the spectra. This may affect the accuracy of T_1 calculations. Therefore, the other three regions (I, III, and V) were used to compare the T_1 changes in paclitaxel signals (neat versus in the SIBS mixture). The relatively lower $T_{1\rho H}$ values of paclitaxel signals in the mixture indicated that the paclitaxel molecule is less densely packed in the SIBS mixture in comparison to the crystalline-packed structure of paclitaxel.

The results show that in general T_1 values decreased for paclitaxel in the paclitaxel–SIBS mixture. This is consistent with restricted molecular motions in the crystalline state, having correlation times comparable to the more isotropic motions occurring in the amorphous state of the mixture (Menger et al., 1982). The longer carbon T_1 is observed for the crystalline state compared to the amorphous state, which indicates that internal molecular mobility of the paclitaxel in the mixture is influenced by interactions with the SIBS main chain.

In the neat paclitaxel sample, the crystal packing and intermolecular H-bonding restricts the mobility of paclitaxel molecules resulting in longer T_1. When paclitaxel is mixed with SIBS, the paclitaxel molecule displayed increased mobility (shorter T_1), due to non-crystal packing of paclitaxel molecule and interference by SIBS. The SIBS-bound paclitaxel molecules tend to follow the internal motions of the polymer chain.

Furthermore, Fig. 8 shows the $T_{1\rho H}$ measurement for paclitaxel–SIBS (1:2, w/w) mixture. The $T_{1\rho H}$ values for the neat samples of paclitaxel and SIBS are summarized in Table 2. Rotating frame proton spin-lattice relaxation time $T_{1\rho H}$, characterizes molecular chain motions in the kilohertz frequency range, and is designed to probe the changes in the interfacial dynamics in the paclitaxel–SIBS mixture in order to provide secondary evidence concerning the morphology of the organic molecules at the polymer interface.

Fig. 9 shows proton $T_{1\rho H}$ data of selected paclitaxel carbon (aliphatic carbons, carbonyl carbon signals at 21 ppm, 75 ppm, and 169 ppm, respectively) intensities plotted as a function of spin-lock times (ms) for the neat and mixed paclitaxel samples. The exponential decay of the neat paclitaxel and mixed paclitaxel data can be represented by a single relaxation time, indicating that a homogeneous system was observed for both. This also indicates homogeneous sample preparation of the paclitaxel–SIBS mixture. Combined with the broad ^{13}C signals of paclitaxel molecule observed in the ^{13}C CP/MAS spectra (Fig. 7), the data suggest

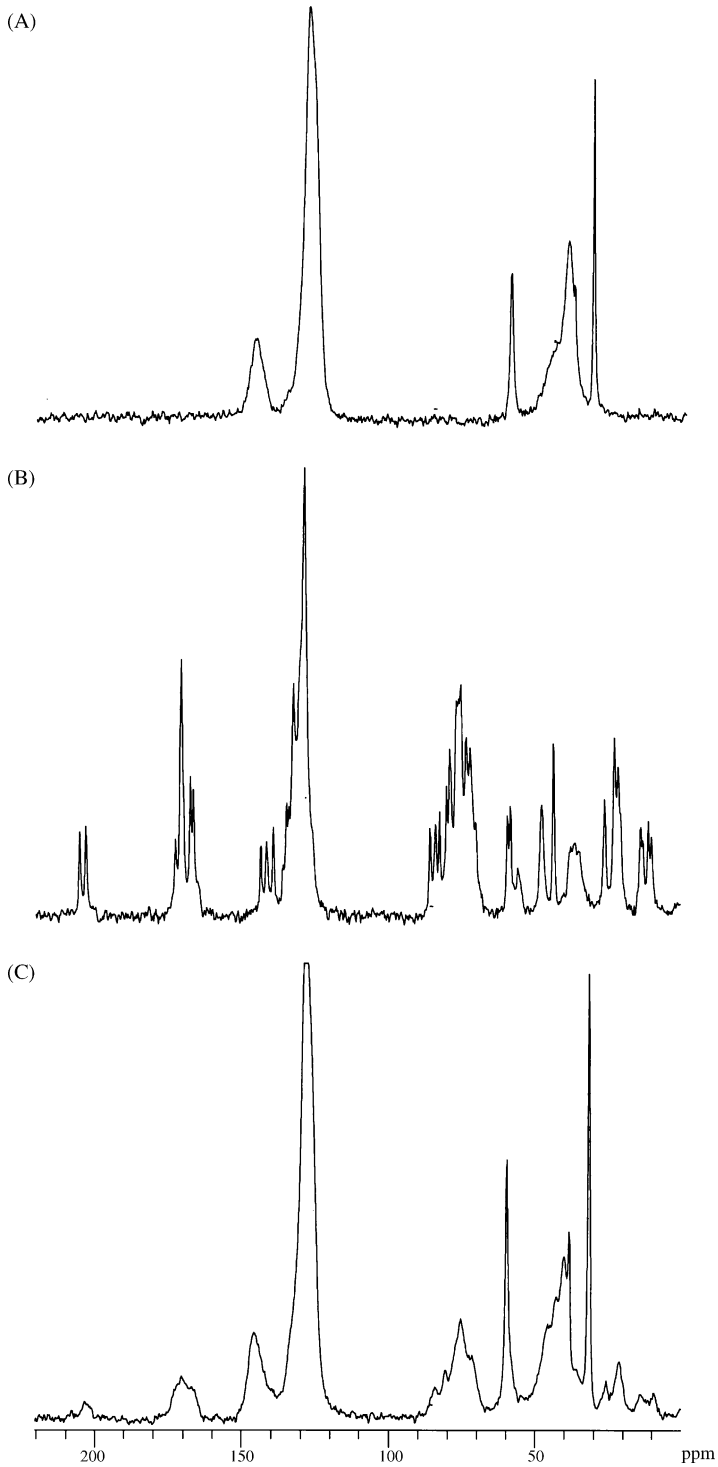

Fig. 7. Solid-state CP/MAS NMR spectra of (A) SIBS with 2048 acquisitions, (B) paclitaxel with 2048 acquisitions, and (C) mixture paclitaxel–SIBS (1:2) with 10,240 acquisitions. All spectra were measured at 298 K with magic-angle spin-rate of 10 kHz.

Table 2
^{13}C chemical shifts of solution NMR and solid-state NMR CP/MAS, ^{13}C T_1 and $T_{1\rho H}$ of solid-state NMR for the samples paclitaxel, SIBS and mixture paclitaxel/SIBS

Carbons	Solution NMR	^{13}C Solid-state CP/MAS NMR								
	Paclitaxel	Paclitaxel			Paclitaxel/SIBS (1:2, w/w)			SIBS		
	^{13}C (ppm)	^{13}C (ppm)	T_1 (s)	$T_{1\rho H}$ (ms)	^{13}C (ppm)	T_1 (s)	$T_{1\rho H}$ (ms)	^{13}C (ppm)	T_1 (s)	$T_{1\rho H}$ (ms)
C-9	203.57	205.7	35.6	14.4	202.9	47.6	9			
		203.5	35.6	14.4						
C-l′	172.63	172.8	79	14.5	172.3	41.2	10.2			
C-30	171.18	170.8	79	14.5	169.5	41.2	11.7			
C-21	167.14									
C-5′	166.87	166.9	42	13.9	166.9	33.3	11.6			
		165.2	42	13.9			10			
					146.4	46.6	8.6	146.1	52.9	9
C-12	141.88	143.8	87.3	11.4						
		141.9	87.3	11.8						
C-38	137.94	139.5	60.5	11.5						
		136.1	55							
C-25	133.64	134.8	38.8							
C-11	133.07	133.5	34.8							
C-41	131.88	132.5	51.5	14.1						
C-24, 26	128.66	128.6	39.7	14.6	128.2	21.8	9.6	128	28.8	8.6
C-5	84.33	85.8	88.7	15.3	85	31.7	12.7			
		84	70.2	15.3	83.9	44	13.4			
C-4	81.04	82.7	79.2	15.2			13.5			
		80.2	76.3		80.9	35.3	12.7			
C-l	78.88	79.1	48.9	14.9						
C-20	76.42	76.8	57.4		76.8	28.3				
C-10	75.51	75.9	50.6	15.4			12.9			
		75.2	49.7	15.4						
C-2′	73.16	73.6	55.1	15.3	73.4	29.5				
C-13	72.15	72.1	39.4	15.5			12.6			
C-7	72.06	69.2	40.3		69.2	30.6				
					60	0.12		60.1	0.29	6
C-8	58.47	59.3	41.5	13.8			5.9			
		58.3	35.6	138						
C-3′	55.06	55.8	43.7	16.1						
C-3	45.61	47.6	84	15.9	45.9	32.3				
C-15	43.09	43.5	11.5	138	43.2	33.8	9.2			
					40.5	36.9	8.5	40.6	43.7	8.5
C-6	35.62	37.6	82.5	18.8	38.7	36.8	8.6			
C-14	35.58	36.2	38.4	18.7						
		35	36.4	18.7						
					31.9	0.52	2.0	32	0.48	1.8
C-17	26.76	26	11.7	13.8	26.1	8.31	12.7			
C-29	22.53	22.7	11.6	13.8						
C-16	21.75	21.2	7.54	13.8	21.6	2.49	12.3			
C-18	14.75	13.7	15.2	12.4	15.6	10.8				
		12.9	20.9	12.7	13.8	10.8	10.1			
C-19	9.52			10.9	10.1	2.83	10.6			

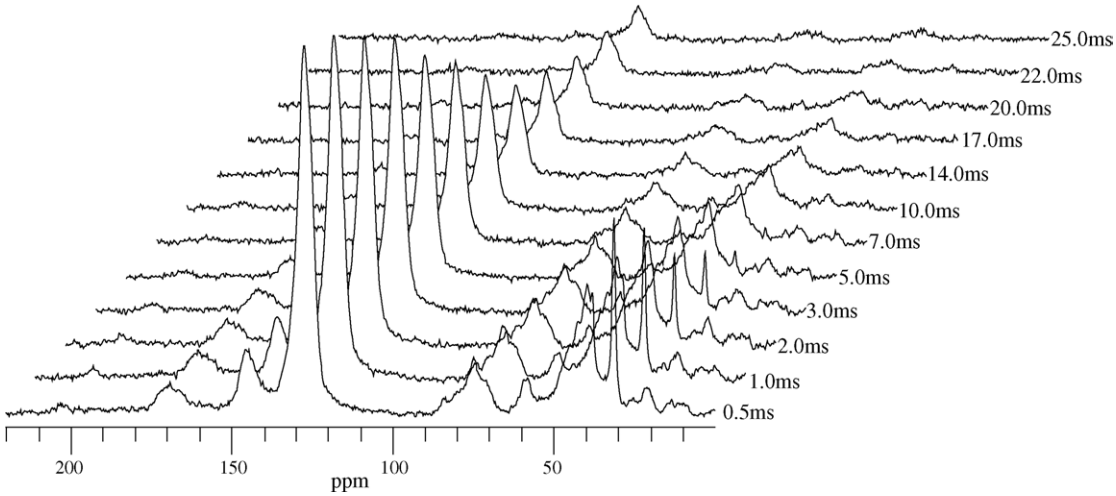

Fig. 8. Stack plot of solid-state NMR proton $T_{1\rho H}$ of paclitaxel–SIBS mixture (1:2, w/w). Each spectrum is a result of 4048 acquisitions at 298 K with magic-angle spin-rate of 10 kHz.

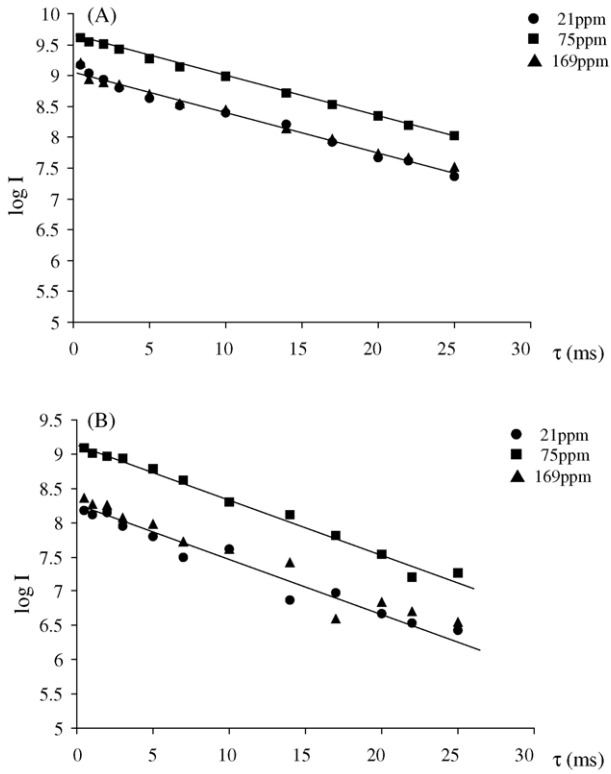

Fig. 9. Proton $T_{1\rho H}$ plot of the peak intensities of the carbon resonances at 21 ppm, 75 ppm, and 169 ppm as a function of spin-lock times (ms) for neat paclitaxel (A) and paclitaxel–SIBS mixture (B); log *I* is the logarithm of the peak intensity.

that paclitaxel in the mixture exists in a non-crystalline amorphous state.

4. Summary

On the basis of our systematic solution and solid-state NMR studies, we conclude that there is no significant chemical change in the paclitaxel molecule when mixed with SIBS in solution and solid states. In other words, there is no NMR-detectable new chemical bond formation between paclitaxel and SIBS. Spin-lattice relaxation time measurements showed shorter T_1 (^{13}C) and $T_{1\rho H}$ measurements for the paclitaxel in the mixture compared to neat paclitaxel, indicating increased mobility for paclitaxel in the paclitaxel–SIBS mixture. The results suggest a change from crystalline packing to amorphous state due to aromatic π–π interactions between paclitaxel and SIBS.

Acknowledgement

This project was funded by Boston Scientific Corporation, USA.

References

Belotti, D., Vergani, V., Drudis, T., Borsotti, P., Pitelli, M.R., Viale, G., Giavazzi, R., Taraboletti, G., 1996. The microtubule-affecting drug paclitaxel has antiangiogenic activity. Clin. Cancer Res. 2, 1843–1849.

Andrew, E.R., 1981. Magic angle spinning in solid state n.m.r. spectroscopy. Phil. Trans. R. Soc. Lond. A 299, 505–520.

Blagosklonny, M.V., Darzynkiewicz, Z., Halicka, H.D., Pozarowski, P., Demidenko, Z.N., Barry, J.J., Kamath, K.R., Herrmann, R.A., 2004. Paclitaxel induces primary and postmitotic G1 arrest in human arterial smooth muscle cells. Cell Cycle 3, 1050–1056.

Chen, S.-H., Wei, J.-M., Farina, V., 1993. Taxol structure-activity relationship: synthesis and biological evaluation of 2-deoxytaxol. Tetrahedron Lett. 34, 3205–3206.

Chieffo, A., Colombo, A., 2004. Polymer-based paclitaxel-eluting coronary stents clinical results in de novo lesions. Herz 29, 147–151.

Chmurny, G.N., Hilton, B.D., Brobst, S., Look, S.A., Witherup, K.M., Beutler, J.A., 1992. Proton and carbon-13 NMR assignments for Taxol, 7-epi-Taxol, and cephalomannine. J. Nat. Prod. 55, 414–423.

Grube, E., Silber, S., Hauptmann, K.E., Mueller, R., Buellesfeld, L., Gerckens, U., Russell, M.E., 2003. TAXUS I: six- and twelve-month results from a randomized double-blind trial on a slow-release paclitaxel-eluting stent for de novo coronary lesions. Circulation 107, 38–42.

Guenard, D., Gueritte-Voegelein, F., Dubois, J., Potier, P., 1993a. Structure–activity relationships of taxol and taxotere analogues. J. Natl. Cancer Inst. Monogr. Field, 79–82.

Guenard, D., Gueritte-Voegelein, G., Potier, P., 1993b. Taxol and taxotere: discovery, chemistry, and structure–activity relationships. Acc. Chem. Res. 26, 160–167.

Harper, J.K., Barich, D.H., Heider, E.M., Grant, D.M., Franke, R.R., Johnson, J.H., Zhang, Y., Lee, P.L., Von Dreele, R.B., 2005. A combined solid state NMR and X-ray powder diffraction study of a stable polymorph of paclitaxel. Cryst. Growth Des. 5, 1737–1742.

Harper, J.K., Facelli, J.C., Barich, D.H., McGeorge, G., Mulgrew, A.E., Grant, D.M., 2002. ^{13}C NMR investigation of solid-state polymorphism in 10-deacetyl baccatin III. J. Am. Chem. Soc. 124, 10589–10595.

Hartmann, S.R., Hahn, E.L., 1962. Nuclear double resonance in the rotating frame. Phys. Rev. 128, 2042–2053.

Jordan, M.A., Toso, R.J., Thrower, D., Wilson, L., 1993. Mechanism of mitotic block and inhibition of cell proliferation by taxol at low concentrations. Proc. Natl. Acad. Sci. U.S.A. 90, 9552–9556.

Jordan, M.A., Wilson, L., 2004. Microtubules as a target for anticancer drugs. Nat. Rev. Cancer 4, 253–265.

LaPlante, S.R., Aubry, N., Deziel, R., Ni, F., Xu, P., 2000. Transferred ^{13}C T1 relaxation at natural isotopic abundance: a practical method for determining site-specific changes in ligand flexibility upon binding to a macromolecule. J. Am. Chem. Soc. 122, 12530–12535.

Li, Y., Poliks, B., Cgelski, L., Poliks, M., Gryczynski, Z., Piszczek, G., Jagtap, P.G., Studelska, D.R., Kingston, D.G.I., Schaefer, J., et al., 2000. Conformation of microtubule-bound paclitaxel determined by fluorescence spectroscopy and REDOR NMR. Biochemistry 39, 281–291.

Mastropaolo, D., Camerman, A., Luo, Y., 1995. Crystal and molecular structure of paclitaxel (Taxol). Proc. Natl. Acad. Sci. U.S.A. 92, 6920–6924.

Menger, E.M., Veeman, W.S., De Boer, E., 1982. Carbon-13 spin-lattice relaxation in solid poly(oxymethylene). Macromolecules 15, 1406–1411.

Moyna, G., Williams, H.J., Scott, A.I., Ringel, I., Gorodetsky, G., Swindell, C.S., 1997. Conformational studies of paclitaxel analogs modified at the C-2′ position in hydrophobic and hydrophilic solvent systems. J. Med. Chem. 40, 3305–3311.

Neagu, C., Puskas, J.E., Singh, M.A., Natansohn, A., 2000. Domain sizes determination for styrene-isobutylene block copolymer systems using solid-state NMR spectroscopy. Macromolecules 33, 5976–5981.

Pines, A., Gibby, M.G., Waugh, J.S., 1973. Proton-enhanced NMR of dilute spins in solids. J. Chem. Phys. 59, 569–590.

Ranade, S.V., Miller, K.M., Richard, R.E., Chan, A.K., Allen, M.J., Helmus, M.N., 2004. Physical characterization of controlled release of paclitaxel from the TAXUS Express 2TM Drug Eluting Stent. J. Biomed. Mater. Res. 71A, 625–634.

Ranade, S.V., Richard, R.E., Helmus, M.N., 2005. Styrenic block copolymers for biomaterial and drug delivery applications. Acta Biomaterialia 1, 137–144.

Schaefer, J., Stejskal, E.O., Buchdahl, R., 1977. Magic-angle carbon-13 NMR analysis of motion in solid glassy polymers. Macromolecules 10, 384–405.

Schiff, P.B., Fant, J., Horwitz, S.B., 1979. Promotion of microtubule assembly in vitro by taxol. Nat. Field 277, 665–667.

Schmidt-Rohr, K., 1995. Multidimensional NMR spectroscopy of polymers. Section overview. ACS Symp. Ser. 598, 184–190.

Stone, G.W., Ellis, S.G., Cox, D.A., Hermiller, J., O'Shaughnessy, C., Mann, J.T., Turco, M., Caputo, R., Bergin, P., Greenberg, J., et al., 2004a. One-year clinical results with the slow-release, polymer-based paclitaxel-eluting TAXUS stent: the TAXUS-IV trial. Circulation 109, 1942–1947.

Stone, G.W., Ellis, S.G., Cox, D.A., Hermiller, J., O'Shaughnessy, C., Mann, J.T., Turco, M., Caputo, R., Bergin, P., Greenberg, J., et al., 2004b. A polymer-based paclitaxel-eluting stent in patients with coronary artery disease. N. Engl. J. Med. 350, 221–231.

Storey, R.F., Chisholm, B.J., Choate, K.R., 1994. Synthesis and characterization of PS-PIB-PS triblock copolymers. J. Macromol. Sci. Pure Appl. Chem. A31, 969–987.

Sullivan, M.J., Maciel, G.E., 1982. Spin dynamics in the carbon-13 nuclear magnetic resonance spectrometric analysis of coal by cross polarization and magic-angle spinning. Anal. Chem. 54, 1615–1623.

Tishmack, P.A., Gugay, D.E., Byrn, S.R., 2003. Solid-state nuclear magnetic resonance spectroscopy—pharmaceutical application. J. Pharm. Sci. 92, 441–474.

Voelker, R., 1991. In: Mathias, L.J. (Ed.), Solid State NMR of Polymers. Plenum Press, New York, pp. 233–244.

Zhu, L., Kurian, E., Prendergast, F.G., Kemple, M.D., 1999. Dynamics of palmitic acid complexed with rat intestinal fatty acid binding protein. Biochemistry 38, 1554–1561.